Three-Dimensional PtRu Nanostructures

Xiaowei Teng, Sean Maksimuk, Samuel Frommer, and Hong Yang*

Department of Chemical Engineering, University of Rochester, Gavett Hall 206, Rochester, New York 14627-0166

Received August 22, 2006. Revised Manuscript Received October 29, 2006

This paper presents an approach to the synthesis of PtRu nanostructures with defined shapes. Platinum acetylacetonate and ruthenium acetylacetonate were used as metal precursors. The selected capping of different low indexed surfaces by adamantaneacetic acid and hexadecaneamine led to the formation of cubic or tetrahedral nanodendrites from faceted primary nanoparticles, most likely through the oriented attachment. Our energy dispersive X-ray (EDX) analysis and X-ray diffraction pattern indicate that the nanostructures were Pt rich and contained up to ∼22 atom % of Ru. These PtRu nanostructures were catalytically active in the direct methanol oxidation. The highest peak mass current density obtained for as-made $Pt_{78}Ru_{22}$ nanodendrites was 99 mA mg^{-1} Pt.

Introduction

This paper describes the synthesis of three-dimensional PtRu alloy nanostructures with controllable shape, texture, and composition. This synthesis relies on the formation of faceted small primary nanoparticles (PNPs) and the subsequent growth of PNPs along the directions defined by the crystal orientation. The as-made nanostructures of PtRu alloys show relatively high catalytic activity toward the oxidation of methanol.

Platinum-based nanoparticles are important electrochemical catalysts for proton exchange membrane fuel cells (PEMFC).[1−4] Designing low cost and highly active catalysts is a challenging and attractive research area despite the considerable advances that have been made in recent years.[1,2,5−7] In comparison to pure platinum, bimetallic PtRu alloys have shown better electrochemical activities in direct methanol oxidation and other similar reactions.[1,8−14] The superior catalytic properties of PtRu nanoparticles can partially be attributed to the ability of platinum atoms in adsorbing and activating methanol in the dehydrogenation steps and neighboring ruthenium atoms in providing the necessary active sites for reaction intermediates to complete the oxidation.[3,14−16] Depending on the synthetic procedure and post-synthesis treatment, the PtRu nanoparticles could have different degrees of crystallinity and surface compositions, which could affect the catalytic property even for those nanoparticles with similar overall composition and average size.

Platinum ruthenium alloy nanoparticles have been prepared via impregnation or arc melting, although the size distribution is broad and the composition varies depending on the methods used.[1,2,17] For low Pt-loading nanostructures, underpotential deposition (UPD) of Pt on less noble metals has been shown to be an effective approach.[18] Spontaneous deposition of a submonolayer of Pt on a Ru nanoparticle surface has been achieved using the UPD method.[18d] Such

* To whom correspondence should be addressed. E-mail: hongyang@che.rochester.edu.

(1) Wieckoweski, A.; Savinova, E. R.; Vayenas, E. G. *Catalysis and Electrocatalysis at Nanoparticle Surface*; Marcel Dekker, Inc.: New York, 2003.
(2) Vielstich, W.; Lamm, A.; Gasteiger, H. A. *Handbook of Fuel Cells: Fundementals Technology and Applications*; John Wiley & Sons, Inc.: Chichester, 2005; Vol. 2.
(3) Hamnett, A. *Catal. Today* **1997**, *38*, 445.
(4) Reddington, E.; Sapienza, A.; Gurau, B.; Viswanathan, R.; Sarangapani, S.; Smotkin, E. S.; Mallouk, T. E. *Science* **1998**, *280*, 1735.
(5) Casado-Rivera, E.; Volpe, D. J.; Alden, L.; Lind, C.; Downie, C.; Vazquez-Alvarez, T.; Angelo, A. C. D.; DiSalvo, F. J.; Abruna, H. D. *J. Am. Chem. Soc.* **2004**, *126*, 4043.
(6) Fernandez, J. L.; Walsh, D. A.; Bard, A. J. *J. Am. Chem. Soc.* **2005**, *127*, 357.
(7) Bardi, U. *Rep. Prog. Phys.* **1994**, *57*, 939.
(8) Chan, K.-Y.; Ding, J.; Ren, J.; Chen, S.; Tsang, K. Y. *J. Mater. Chem.* **2004**, *14*, 505.
(9) (a) Maillard, F.; Lu, G. Q.; Wieckowski, A.; Stimming, U. *J. Phys. Chem. B* **2005**, *109*, 16230. (b) Waszczuk, P.; Solla-Gullon, J.; Kim, H. S.; Tong, Y. Y.; Montiel, V.; Aldaz, A.; Wieckowski, A. *J. Catal.* **2001**, *203*, 1.
(10) (a) Wang, L. L.; Khare, S. V.; Chirita, V.; Johnson, D. D.; Rockett, A. A.; Frenkel, A. I.; Mack, N. H.; Nuzzo, R. G. *J. Am. Chem. Soc.* **2006**, *128*, 131. (b) Hills, C. W.; Nashner, M. S.; Frenkel, A. I.; Shapley, J. R.; Nuzzo, R. G. *Langmuir* **1999**, *15*, 690. (c) Hills, C. W.; Mack, N. H.; Nuzzo, R. G. *J. Phys. Chem. B* **2003**, *107*, 2626. (d) Nashner, M. S.; Frenkel, A. I.; Somerville, D.; Hills, C. W.; Shapley, J. R.; Nuzzo, R. G. *J. Am. Chem. Soc.* **1998**, *120*, 8093.
(11) Gurau, B.; Viswanathan, R.; Liu, R. X.; Lafrenz, T. J.; Ley, K. L.; Smotkin, E. S.; Reddington, E.; Sapienza, A.; Chan, B. C.; Mallouk, T. E.; Sarangapani, S. *J. Phys. Chem. B* **1998**, *102*, 9997.
(12) Iwasita, T.; Hoster, H.; John-Anacker, A.; Lin, W. F.; Vielstich, W. *Langmuir* **2000**, *16*, 522.
(13) Takasu, Y.; Fujiwara, T.; Murakami, Y.; Sasaki, K.; Oguri, M.; Asaki, T.; Sugimoto, W. *J. Electrochem. Soc.* **2000**, *147*, 4421.
(14) Watanabe, M.; Motoo, S. *J. Electroanal. Chem.* **1975**, *60*, 267.
(15) Chu, D.; Gilman, S. *J. Electrochem. Soc.* **1996**, *143*, 1685.
(16) Lu, C.; Rice, C.; Masel, R. I.; Babu, P. K.; Waszczuk, P.; Kim, H. S.; Oldfield, E.; Wieckowski, A. *J. Phys. Chem. B* **2002**, *106*, 9581.
(17) (a) Gasteiger, H. A.; Markovic, N.; Ross, P. N.; Cairns, E. J. *J. Phys. Chem.* **1994**, *98*, 617. (b) Gasteiger, H. A.; Markovic, N.; Ross, P. N.; Cairns, E. J. *J. Electrochem. Soc.* **1994**, *141*, 1795. (c) Gasteiger, H. A.; Ross, P. N.; Cairns, E. J. *Surf. Sci.* **1993**, *293*, 67.
(18) (a) Zhang, J. L.; Vukmirovic, M. B.; Xu, Y.; Mavrikakis, M.; Adzic, R. R. *Angew. Chem., Int. Ed.* **2005**, *44*, 2132. (b) Zhang, J.; Mo, Y.; Vukmirovic, M. B.; Klie, R.; Sasaki, K.; Adzic, R. R. *J. Phys. Chem. B* **2004**, *108*, 10955. (c) Zhang, J.; Lima, F. H. B.; Shao, M. H.; Sasaki, K.; Wang, J. X.; Hanson, J.; Adzic, R. R. *J. Phys. Chem. B* **2005**, *109*, 22701. (d) Brankovic, S. R.; Wang, J. X.; Adzic, R. R. *Electrochem. Solid State Lett.* **2001**, *4*, A217.

10.1021/cm061979b CCC: $37.00
Published on Web 12/07/2006

catalysts have shown good CO tolerance at low platinum loading. Besides the above approaches, colloidal synthesis is becoming a very useful alternative for making PtRu alloy nanoparticles. A high level of control over size, shape, and chemical composition can be possible for PtRu catalysts through the solution-phase synthesis.[1,2,15,19,20] Although many efforts have been devoted to the development of such nanoparticles, most of the work has focused on the non-textured form. Design and synthesis of a porous or highly interconnected network of PtRu alloy nanoparticles can potentially create new opportunities for making high-performance catalysts.

Porous or flower-shaped nanomaterials of metals and metal oxides have recently been made by several groups.[21−27] There are two major strategies for making this type of platinum nanostructures. One is to use lyotropic liquid crystal or lipid membrane as the template to generate porous structures.[25−27] Mesostructured materials and dendritic sheets of platinum have been made. Jiang and Kucernak have shown the synthesis of microspheres of mesoporous PtRu alloys by reducing hexachloroplatinic acid and ruthenium trichloride in the hydrophilic domains of oligoethylene oxide lyotropic liquid crystals, similar to the templating methods.[26]

An approach to the synthesis of porous Pt nanoparticles through the polyol process has been reported recently.[22] This method did not rely on the formation of supramolecular templates but was related to the oriented attachment of PNPs between the surfaces with similar atomic structures. Nano-flowers of metal oxides have also been made recently by this strategy.[21] In this paper, we show PtRu alloys can be made as three-dimensional (3D) nanostructures that have not only textures but also definable shapes, suggesting the 3D structures form due to the dendritic growth of PNPs based on the oriented attachment principle.

Experimental Section

Synthesis. In a typical procedure, platinum acetylacetonate ($Pt(acac)_2$, Gelest Inc., 97%, 50 mg), ruthenium acetylacetonate ($Ru(acac)_3$, Aldrich, 97%, 50 or 100 mg), diphenyl ether (DPE, Aldrich, 99%, 2 mL), 1-adamantaneacetic acid (AAA, Aldrich, 99%, 150 or 220 mg), and hexadecaneamine (HDA, Aldrich, 90%, 4 g) were added into a 25 mL three-neck round-bottom flask. This reaction mixture was heated to 190 °C using a heating mantle at a rate of 10 °C/min. In a separate setup, a mixture of 1, 2-hexadecanediol (HDD, Aldrich, 90%, 1 or 1.43 g) was dissolved in 2 mL of DPE at 130 °C and subsequently injected into the flask containing $Pt(acac)_2$ and $Ru(acac)_3$. The color of the solution turned from dark red to dark black spontaneously. The reaction was maintained at the reflux temperature (280 °C) for 30 min. After the reaction, the nanoparticles were separated and washed using chloroform and ethanol, respectively. In a typical procedure, 200 μL of the product was dispersed in 800 μL of chloroform in a plastic vial (2 mL), followed by the addition of 1 mL of ethanol, which was used as the anti-solvent. The precipitate was separated from the solution mixture by a centrifuge at 6000 rpm for 7 min. Yellow-brownish supernatant was decanted, and the black product was dispersed in 1 mL of chloroform. This process was repeated three times.

Characterizations. Electron microscope specimens were prepared by dispersing the suspension of nanoparticle in chloroform (~1 mg/mL) and drop-casting it onto TEM grids. The transmission electron microscopy (TEM) images were recorded on a JEOL JEM 1200EX microscope at an accelerating voltage of 120 kV. Energy dispersive X-ray (EDX) analysis was obtained with a field-emission scanning electron microscope (FE-SEM, model LEO 982) equipped with an EDAX detector or a Hitachi HD-2000 scanning transmission electron microscope (STEM) equipped with the EDX system from Oxford Instruments, Inc. that has a lateral resolution of 0.18 nm. The high-resolution TEM (HR-TEM) images were recorded on a FEI Tecnai G20 microscope at an accelerating voltage of 200 kV. Powder X-ray diffraction (PXRD) patterns were taken using a Philips MPD diffractometer with a Cu Kα X-ray source ($\lambda = 1.5405$ Å) at a scan rate of 0.013° 2θ/s. The X-fit and Treor were used to obtain the lattice constant, full width at half-maximum (FWHM), and lattice spacing. The particle size distribution was obtained by analyzing about 100 particles on TEM images using the ImageJ software from NIH.

Electrocatalytic Study. The electrochemical catalytic activities of PtRu nanostructures were characterized using a three-electrode system on a CHI 760 dual channel electrochemical workstation (CH Instruments, Inc). A platinum wire was used as the counter electrode, and an Ag/AgCl (3 M KCl) electrode was the reference. The working electrode was made of glassy carbon that was polished with Al_2O_3 powders (Aldrich, 1 μm) and rinsed with Millipore deionized water prior to the test. Cyclic voltammetry (CV) was conducted in the supporting electrolyte for multiple cycles until a stable curve was obtained. All the solutions were prepared using Millipore deionized water. Perchloric acid ($HClO_4$, Aldrich, 99.999%, 0.1 M) was used as the supporting electrolyte. Methanol (CH_3OH, anhydrous) was the analytical reagent from Aldrich. All solutions were deaerated with argon for at least 15 min before the measurements. A 10 μL dispersion of PtRu catalysts, which was prepared by sonicating nanoparticles in ethanol (0.5 mg Pt mL^{-1}) for 10 s, was drop-cast onto a carbon electrode (5 mm in diameter). The CV was performed at 22 °C, and the variation of temperature was controlled within ±0.1 °C using a circulating bath (Polyscience, model 1180A). The potential was swept between 0 and 1 V at a rate of 50 mV s^{-1}. The rate of the rotating disk electrode (working electrode) was set at 1000 rpm for the measurements. The chronoamperometry of PtRu nanoparticles was recorded at a bias voltage of 0.6 V. The change in the current density with time was recorded for 100 min. The loading amount of PtRu catalysts was 25 μg cm^{-2} for all the measurements. The activation energy was obtained from the slope of the Arrhenius relationship, in which $\log(i, \text{A cm}^{-2})$ was plotted against $1000/T$, where i is current density

(19) (a) Bock, C.; MacDougall, B.; LePage, Y. *J. Electrochem. Soc.* **2004**, *151*, A1269. (b) Bock, C.; Paquet, C.; Couillard, M.; Botton, G. A.; MacDougall, B. R. *J. Am. Chem. Soc.* **2004**, *126*, 8028.
(20) (a) Liu, Z. L.; Ling, X. Y.; Su, X. D.; Lee, J. Y. *J. Phys. Chem. B* **2004**, *108*, 8234. (b) Liu, Z. L.; Lee, J. Y.; Chen, W. X.; Han, M.; Gan, L. M. *Langmuir* **2004**, *20*, 181. (c) Deivaraj, T. C.; Lee, J. Y. *J. Power Sources* **2005**, *142*, 43.
(21) (a) Narayanaswamy, A.; Xu, H.; Pradhan, N.; Kim, M.; Peng, X. *J. Am. Chem. Soc.* **2006**, *128*, 10310. (b) Narayanaswamy, A.; Xu, H.; Pradhan, N.; Peng, X. *Angew. Chem., Int. Ed.* **2006**, *45*, 5361.
(22) Teng, X. W.; Liang, X. Y.; Maksimuk, S.; Yang, H. *Small* **2006**, *2*, 249.
(23) Wang, Z.; Qian, X. F.; Yin, J.; Zhu, Z. K. *Langmuir* **2004**, *20*, 3441.
(24) Zhong, X.; Feng, Y.; Lieberwirth, I.; Knoll, W. *Chem. Mater.* **2006**, *18*, 2468.
(25) Attard, G. S.; Bartlett, P. N.; Coleman, N. R. B.; Elliott, J. M.; Owen, J. R.; Wang, J. H. *Science* **1997**, *278*, 838.
(26) (a) Jiang, J. H.; Kucernak, A. *J. Electroanal. Chem.* **2003**, *543*, 187. (b) Jiang, J. H.; Kucernak, A. *Chem. Mater.* **2004**, *16*, 1362.
(27) (a) Song, Y. J.; Yang, Y.; Medforth, C. J.; Pereira, E.; Singh, A. K.; Xu, H. F.; Jiang, Y. B.; Brinker, C. J.; van Swol, F.; Shelnutt, J. A. *J. Am. Chem. Soc.* **2004**, *126*, 635. (b) Song, Y. J.; Steen, W. A.; Pena, D.; Jiang, Y. B.; Medforth, C. J.; Huo, Q. S.; Pincus, J. L.; Qiu, Y.; Sasaki, D. Y.; Miller, J. E.; Shelnuttt, J. A. *Chem. Mater.* **2006**, *18*, 2335.

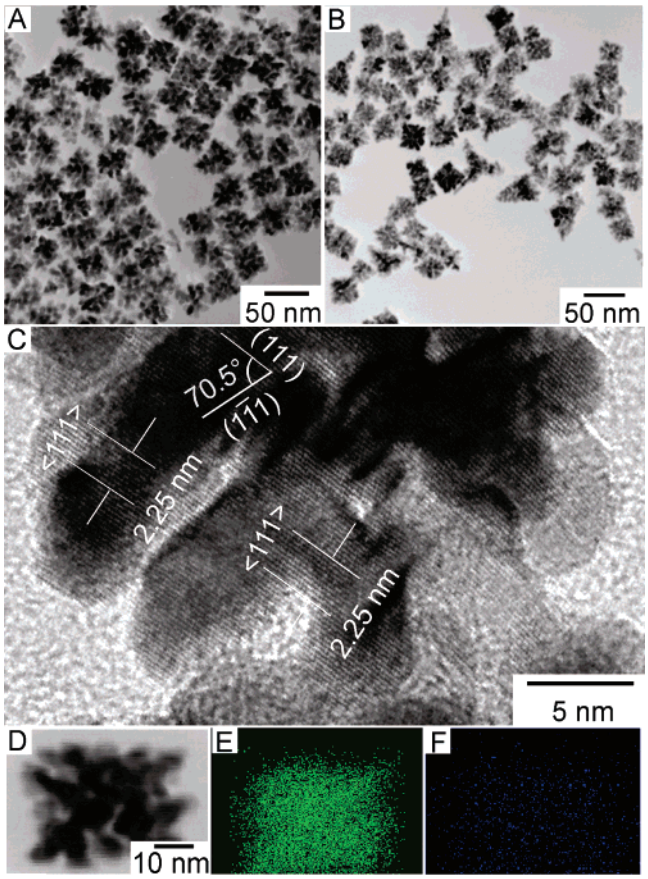

Figure 1. TEM images of PtRu nanodendrites made at $Pt(acac)_2/Ru(acac)_3$/AAA/HDD molar ratio of (A) 1:1:6:30 and (B) 1:2:9:45, respectively; (C) HR-TEM image of a portion of a cubic PtRu nanodendrite shown in panel A; (D) TEM and (E, F) EDX maps of a single nanodendrite showing the uniformly distributed (E) Pt and (F) Ru elements. The HDA/DPE molar ratio was kept at 120:200.

and *T* is temperature. The temperature range was between 25 and 60 °C. The peak mass current density presented was after baseline correction.

Results and Discussion

Figure 1A shows the TEM image of the PtRu nanoparticles made at a $Pt(acac)_2/Ru(acac)_3$/AAA/HDD molar ratio of 1:1:6:30. The molar ratio between HDA and DPE was kept at 120:200 for all the reactions. The nanoparticles formed after the reaction for 30 min at the reflux temperature, which is around 280 °C. The as-made nanoparticles had a relatively uniform cubic shape consisting of interconnected PNPs. The average length of the edges of these cube-shaped nanostructures was 31.1 ± 2.3 nm. The PNPs had an average width around 4.2 nm. Figure 1B shows the TEM image of as-made PtRu nanodendrites when the $Pt(acac)_2/Ru(acac)_3$/AAA/HDD molar ratio was changed to 1:2:9:45. At this reactant ratio the particles had either cubic or tetrahedral symmetry. These two types of morphologies could be the result of growth of PNPs along ⟨111⟩ directions in a dendritic fashion.

The high-resolution TEM image shows that the PNPs in these PtRu nanostructures were single crystalline (Figure 1C)). The lattice spacing was equal to 2.25 Å (or 2.25 nm for 10 consecutive fringes), which could be assigned to the {111} planes of PtRu alloy. The HR-TEM image further shows such well-resolved lattice planes at a 70° angle for neighboring PNPs, further indicating that they were (111) and (1$\bar{1}$1) planes of cubic phase PtRu alloys.[28] Within the cubic shape nanoparticles, the short rod shape could be observed, presumably due to the oriented attachment of PNPs along ⟨111⟩ directions. Such nanoparticle-to-rod transformation also happens for different types of quantum dots.[29] Unlike the cases in CdTe and PbSe quantum dots where the dipole moment was the driving force, the oriented attachment in these PtRu nanostructures was most likely due to the incomplete growth inhibition by capping reagents on selected crystal surfaces.

In general, the shape of nanoparticles is highly dependent on the relative growth rates along the low index crystal planes.[30] These growth rates could be quite different for colloidal nanoparticles in the presence of surfactants. AAA seemed to preferentially adsorb on the {100} surfaces of PtRu and facilitate the growth along ⟨111⟩ directions. Unlike most of the reported cases of nanoflowers, the secondary growth of PNPs apparently took several preferred equivalent directions. The secondary growth of PNPs could be faster along ⟨111⟩ than ⟨100⟩ directions, leading to the formation of cube-shaped nanostructure in a dendritic fashion. By increasing the $Ru(acac)_3$ to $Pt(acac)_2$ ratio and the amount of AAA and HDD, the PNPs could still also grow along ⟨111⟩ directions. In this case, however, the increase in the concentration of capping agents led to a better coverage of the surfaces of nanocrystals. Thus, instead of forming cube-like nanodendrites which grew along eight ⟨111⟩ directions, the PNPs might grow at a reduced numbers of surfaces, leading to the formation of tetrahedral nanodendrites that had four equivalent growth directions.

The composition of individual nanoparticle was investigated by EDX analysis. Figure 1D−F shows the TEM image and the corresponding EDX maps for Pt and Ru elements, respectively, of an individual nanoparticle from the product made at a $Pt(acac)_2/Ru(acac)_3$ molar ratio of 1:1. The Pt and Ru signals were readily detectable, and both elements evenly distributed throughout these nanodendrites. It is noted that the amount of reducing reagent used was about 15 times the total mole number of $Pt(acac)_2$ and $Ru(acac)_3$. Under such a highly reductive environment, platinum and ruthenium cations could be reduced to Pt^0 and Ru^0 rapidly, judging by the rapid color change from dark red to black during the reaction. The obtained atomic ratio was $Pt_{81}Ru_{19}$, which was similar to $Pt_{85}Ru_{15}$ obtained from the EDX data of an ensemble of PtRu nanoparticles. Similar measurements were conducted with the nanoparticles shown in Figure 1B, which had a composition of $Pt_{78}Ru_{22}$ for the ensemble and $Pt_{75}Ru_{25}$ for a single particle. These EDX measurements indicate that the composition of these as-made PtRu nanodendrites was relatively uniform. The yields of $Pt_{85}Ru_{15}$ nanodendrites were about 84% based on the weight of Pt, and $Pt_{78}Ru_{22}$ nanodendrites had a similar yield. These data indicate that

(28) Edington, J. W. *Electron Diffraction in the Electron Microscope*; Macmillan: Eindhoven, 1975.
(29) (a) Tang, Z. Y.; Kotov, N. A. *Adv. Mater.* **2005**, *17*, 951. (b) Tang, Z. Y.; Kotov, N. A.; Giersig, M. *Science* **2002**, *297*, 237. (c) Pradhan, N.; Xu, H. F.; Peng, X. G. *Nano Lett.* **2006**, *6*, 720.
(30) (a) Wang, Z. L. *J. Phys. Chem. B* **2000**, *104*, 1153. (b) Wiley: B.; Sun, Y. G.; Mayers, B.; Xia, Y. N. *Chem.—Eur. J.* **2005**, *11*, 454.

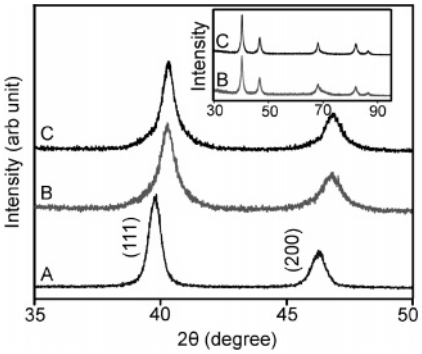

Figure 2. PXRD patterns of (A) Pt nanoparticles and (B) $Pt_{85}Ru_{15}$ and (C) $Pt_{78}Ru_{22}$ nanodendrites. Inset shows the PXRD patterns of the two PtRu nanodendrites between 30 and 95° 2θ.

Table 1. Peak Position, Lattice Spacing, Primary Particle Size, and Unit Cell Constant

source	sample	peak position (2θ, deg)	lattice spacing (Å)	particle size[a] (nm)	unit cell constant (Å)
JCDPS	Pt(111)	39.76	2.265	n/a	3.920
	Pt(200)	46.25	1.962		
PXRD	$Pt_{85}Ru_{15}$(111)	40.23	2.242	5.9	3.884
	$Pt_{85}Ru_{15}$(200)	46.72	1.942		
	$Pt_{78}Ru_{22}$(111)	40.30	2.239	6.7	3.878
	$Pt_{78}Ru_{22}$(200)	46.82	1.939		

[a] Size analysis of PNPs is based on the FWHM of the PtRu (111) peak.

although both $Pt(acac)_2$ and $Ru(acac)_3$ could be reduced effectively at this temperature, the amount of Ru atoms that was incorporated into Pt lattices was limited. The stable colloidal form of alloy between these two metal precursors in this reaction system was close to Pt_3Ru. The differences in reaction rate between these two precursors and the crystalline phase between pure platinum and ruthenium metals could be the main reasons for this limited variation in composition that we could obtain.

Figure 2 shows the PXRD patterns of these two nanodendrites. The PXRD pattern of platinum nanoparticles was included for comparison. The PXRD patterns could be assigned to the (111), (200), (220), (311), and (222) diffractions of face-centered cubic (fcc) PtRu alloys.[20a] The 2θ angles were higher for nanoparticles of PtRu alloys than for pure Pt, as the incorporation of Ru atoms into Pt lattices led to the decrease in the lattice constant. The FWHM of the (111) diffraction was used to estimate the average size of the PNPs according to the Scherrer equation.[22] Table 1 summarizes the peak position, lattice spacing, average particle size, and unit cell constant calculated using the experimental data and JCDPS X-ray diffraction database. The calculated sizes of PNPs based the peak broadening in PXRD data agreed in general with those obtained from the TEM study. X-ray line shape was fit based on pseudo-Voigt (PV) and split Pearson (PVII) functions with a fundamental parameter (FP) convolution approach using XFIT.[31] The peak position and FWHM were obtained from the fits and used to generate lattice parameters, such as interplanar distance and lattice constant based on the Treor analysis. The change in lattice constant could be used to estimate the elemental composition between these two metals assuming that Vegard's law relationship applies to the nanoparticles.[19a]

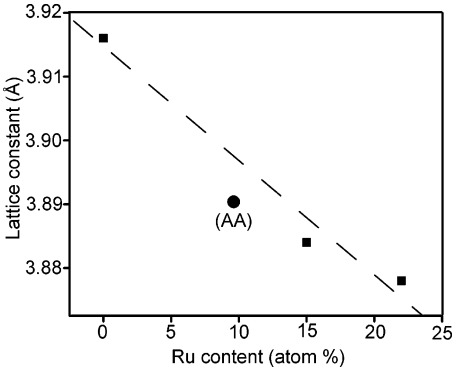

Figure 3. Dependence of the lattice constant on the Ru content (atom %) for $Pt_{100-x}Ru_x$ nanodendrites.

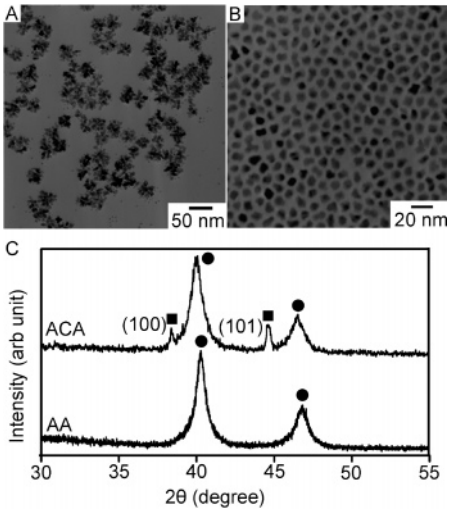

Figure 4. TEM images of as-made PtRu nanoparticles synthesized using (A) ACA and (B) AA as one of the capping agents. (C) PXRD patterns of the corresponding PtRu nanoparticles. Diffractions from both fcc PtRu alloys (●) and hcp Ru metal (■) were observed for the sample when ACA was used. The $Pt(acac)_2/Ru(acac)_3$/ACA or AA/HDD molar ratio was 1:1:6:30.

Figure 3 shows the lattice constants obtained for Pt nanoparticles and $Pt_{85}Ru_{15}$ and $Pt_{78}Ru_{22}$ nanodendrites. The lattice constant decreased almost proportionally as the Ru content increased. The unit cell constant had a linear relationship with Ru content, and the slope was −0.0018 Å, which was comparable to the reported value.[19a] The adamantane moiety appeared to be one of the key functional groups of the capping agents. Adamantanecarboxylic acid (ACA) and adamantanamine (AA) were further tested to examine the effect of such reagents on the morphology and composition of PtRu nanostructures. Figure 4 shows TEM images and PXRD patterns of the nanoparticles when AAA was replaced by either ACA or AA in the reaction mixtures. All other reactants were maintained the same, and the synthetic conditions were also the same as those for making the 31-nm $Pt_{85}Ru_{15}$ cube-shaped nanodendrites, as shown in Figure 1A. The 3D nanostructures were observed only when ACA was used as one of the capping agents. When AA was employed, only faceted nanoparticles were observed. In this case, the as-made nanoparticles had an overall composition close to $Pt_{90}Ru_{10}$. This composition could qualitatively be fit to a linear relationship between the lattice constant and the Ru content for the nanodendrites, Figure 3. We noted

(31) Cheary, R. W.; Coelho, A. A. *J. Appl. Crystallogr.* **1992**, *25*, 109.

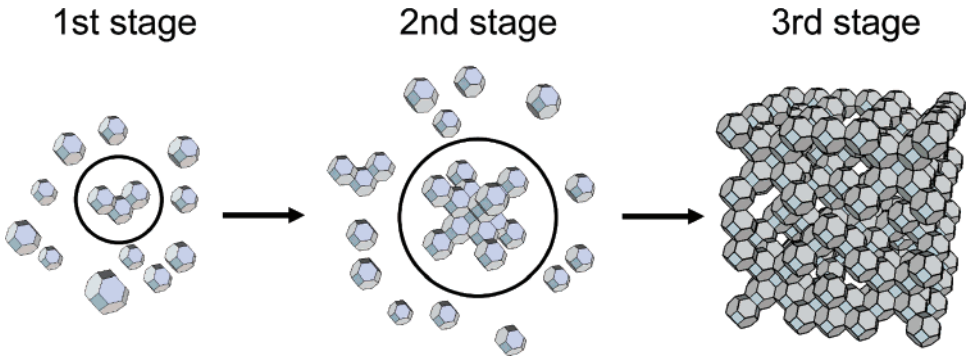

Figure 5. Illustration of the formation of 3D PtRu nanodendrites.

that besides PtRu alloy, nanoparticles of pure Ru could be detected by PXRD when ACA was used as the capping agent, Figure 4C. This observation suggests that the byproducts could be pure Ru nanoparticles. These Ru-nanoparticle byproducts could be readily separated out from PtRu nanodendrites when AAA was used.

The shape of PtRu alloys changed from nanodendrites to faceted nanoparticles when the carboxylic acid functional group was replaced by amine. In a separate control experiment when adamantane-based capping agents were replaced with oleic acid, only aggregates of nearly spherical particles could be obtained. These observations indicate that both adamantane and carboxyl acid groups are essential in the formation of PtRu nanodendrites. Nucleation at the low concentration of $Pt(acac)_2$ and subsequent growth via oriented attachment of PNPs led to the formation of dendrites, as illustrated in Figure 5. Upon the formation of PNPs with defined shapes (Stage 1), the secondary growth happened preferentially at the {111} faces, which were less protected than {100} faces (Stage 2). This oriented growth of PNPs eventually led to the formation of dendritic nanostructures with well-defined morphology (Stage 3).

The catalytic property of $Pt_{85}Ru_{15}$ and $Pt_{78}Ru_{22}$ dendrites for the oxidation of methanol was studied using CV. The observed methanol oxidation peaks for both $Pt_{85}Ru_{15}$ and $Pt_{78}Ru_{22}$ nanodendrites were at 0.63 V (vs Ag/AgCl) in the forward sweep and at 0.51 V in the backward sweep, Figure 6A. The current density per unit mass of platinum was calculated based on the CV recorded after 100 cycles. The peak mass current densities were 99 mA mg^{-1} Pt for $Pt_{78}Ru_{22}$ and 74 mA mg^{-1} Pt for $Pt_{85}Ru_{15}$ nanodendrites. As a reference, a carbon-supported PtRu catalyst (HiSPEC 7000, Johnson Matthey, 30% Pt, 15% Ru, and 55% carbon) was tested, which had a mass current density of 49 mA mg^{-1} Pt. One reason for the high catalytic property could be due to the fact that these nanodendrites had compositions close to $Pt_{70}Ru_{30}$, which is the optimized composition for having the highest catalytic performance toward the methanol oxidation.[23] The chronoamperometry data indicated that the difference in the mass current density for $Pt_{78}Ru_{22}$ and $Pt_{85}Ru_{15}$ dendrites remained almost the same when the reaction reached the steady state after 6000 s, Figure 6B. The activation energy, E_a, determined according to Arrhenius relationship, was 24.8 ± 1.3 kJ mol^{-1} for $Pt_{78}Ru_{22}$ and 27.0 ± 1.5 kJ mol^{-1} for $Pt_{78}Ru_{22}$ nanodendrites, inset of Figure 6B. These values were lower than those of the polycrystalline PtRu electrode (60 kJ mol^{-1})[17b] and mesoporous PtRu electrodes (30−45 kJ mol^{-1})[26a] but comparable to a value of 29 kJ mol^{-1} measured on 15 nm PtRu nanoparticles.[15] The difference in activation energies among these catalysts could be related to the variations in the composition, crystallinity, and surface structure.[1,2] These structural parameters also depended on how the electrodes were prepared including the condition of postsynthetic treatment of nanoparticles, such as temperature and whether carbon supports were used.

The electrochemical oxidation of methanol by PtRu catalysts goes through multiple intermediate steps including the formation of adsorbed CO, CO_{ads}.[2] The dehydrogenation of adsorbed methanol typically happens at Pt atom sites to

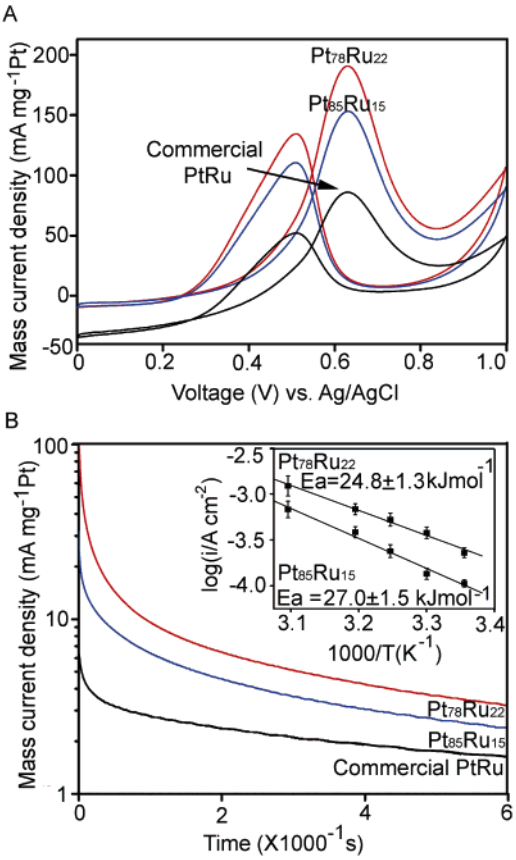

Figure 6. (A) CV and (B) chronoamperometry for methanol oxidation catalyzed by $Pt_{78}Ru_{22}$ and $Pt_{85}Ru_{15}$ nanodendrites and the reference PtRu catalyst (HiSPEC 7000 from Johnson Matthey), respectively. The inset shows the Arrhenius plots using $Pt_{85}Ru_{15}$ and $Pt_{78}Ru_{22}$ nanodendrites as the catalysts.

form CO_{ads}, while Ru atoms provide sites for water adsorption. Typically, the adsorption and decomposition of water on the surface of a catalyst limits the overall rate of the reaction series. Increasing the Ru content can provide more reaction sites and facilitates the oxidation of CO_{ads}. However, the introduction of Ru atoms results in the reduction of surface Pt sites, and the rate-determining step can change to methanol adsorption and dehydrogenation. Thus, a proper Pt/Ru atomic ratio and surface structure are essential to achieve the maximum catalytic performance. The optimal composition of PtRu alloys has been found experimentally to be around $Pt_{70}Ru_{30}$.[17c,19a] The highest amount of Ru that was incorporated into the PtRu alloy nanodendrites in our current work was about 22 atom %. Interestingly, this atomic ratio was close to that for $CoPt_3$ nanoparticles, when HDA and ACA were used as the capping agents under comparable but less reductive reaction conditions.[32] This observation further indicates that the interplay between an adamantane-based capping agent and HDA could not only affect the size and shape but also the composition of Pt-based bimetallic alloys. The dendritic structure which contained pores within the particles might also play a role in determining the catalytic performance.

(32) Shevchenko, E. V.; Talapin, D. V.; Rogach, A. L.; Kornowski, A.; Haase, M.; Weller, H. *J. Am. Chem. Soc.* **2002**, *124*, 11480.

Conclusion

We have developed a new synthetic method for making PtRu alloy nanodendrites with defined 3D shapes. The formation of nanodendrites relies on the secondary growth of PNPs. The fact that lattices at the interface regions of PNPs are matched suggests oriented attachment took place in the formation 3D nanodendrites. The interaction between adamantaneacetic acid and selected surfaces of PtRu PNPs such as {100} faces could facilitate this preferred growth. This template-free approach can be a useful method for making nanoparticles of PtRu and other metal alloys with new structures which can be desirable for catalytic applications.

Acknowledgment. This work was supported in part by U.S. National Science Foundation (DMR-0449849 and CTS-0417722) and the Environmental Protection Agency (EPA-STAR R831722). Acknowledgment is also made to the Donors of the American Chemical Society Petroleum Research Fund for partial support of this research. This work made use of the FEI Tecnai G20 microscope at the Cornell Center for Materials Research (CCMR) supported by NSF (DMR-0520404) and a Hitachi HD-2000 STEM at the Centre for Nanostructure Imaging, University of Toronto, funded by Canada Foundation of Innovation and Ontario Innovation Trust. We thank Dr. John Grazul (Cornell) and Dr. Neil Coombs (University of Toronto) for help.

CM061979B